NJC

PAPER

View Article Online
View Journal | View Issue

Fe-terpyridyl complex based multiple switches for application in molecular logic gates and circuits†‡

Cite this: *New J. Chem.*, 2014, **38**, 2679

Received (in Montpellier, France) 23rd January 2014,
Accepted 24th March 2014

DOI: 10.1039/c4nj00121d

www.rsc.org/njc

Prakash Chandra Mondal,*[ab] Vikram Singh*[a] and Bhaskaran Shankar[a]

Molecular logic gates and circuits are constructed using the optical and electrochemical addressable-reversible-multiple switching event of the Fe(II)-4′-pyridyl terpyridyl complex (**1**) using multiple analytes. The process involves oxidation–reduction of Fe^{2+} as well as successive quaternization–dequaternization of the free pendant pyridyl group monitored optically. The whole switching process could also be visualized by the naked eye as colour changes upon switching are quite apparent and instant.

1 Introduction

Molecular logic has seen exponential growth in recent times.[1–3] A chemical approach towards molecular logic is inherently viable, since molecules are the smallest entities which have discrete shape and properties.[4–6] Molecular manipulation by chemists through a bottom-up approach could probably result in more efficient nanoscale devices, unlike the top-down approach, which has its own intrinsic limitations.[7,8] Generally, molecules which could switch between at least two stable states, upon specific external input(s), have found practical applications in construction of molecular logic gates and circuits. Such intelligent use of inorganic/organic molecules and their interplay with varying input(s) have resulted in the development of information technology at the molecular level.[9] In this context, chemists have utilized and fine-tuned the redox, photophysical and photochemical properties of polypyridyl complexes of transition metal ions such as Fe(II), Ru(II), Ir(III), Os(II) and Re(I) in the overall development of materials science.[10,11] Interestingly, these properties/states could easily be set/reset through external triggers/inputs, *viz.* light, electric field, magnetic field or chemicals, while keeping the molecule stable in different states and often leading to visible colour changes or similar easy to recognize properties as outputs.[12] This fine relationship between molecular properties in different yet stable and identifiable states leads to molecular multiple switches. Such molecule based switches have gained a lot of interest from the scientific community for the development of molecular logic gates in solution as well as on surfaces.[13–19]

Our group has been engaged in exploring the tremendous potential of terpyridyl-transition metal complexes both in solution as well as on solid surfaces.[20–22] Functionalized terpyridyl and its derivatives offer several synthetic and structural advantages due to its excellent structure–property correlations. For example, (i) it has a strong ''chelate effect'' towards the transition metal ions, (ii) a facile synthetic route, (iii) versatile coordination modes and (iv) the strong π-electron accepting nature of the ligand stabilizes the metal ions in lower oxidation states. In the present work, an optically rich and redox-active Fe(II)-terpyridylcomplex (**1**) (Fig. 1) has been utilized for successful demonstration of multiple switching events with chemical(s) and electric potential as input and the process is monitored optically using an off-the-shelf UV-Vis spectrophotometer under transmission mode. These triggered, reversible events prompted us to construct related molecular-integrated molecular logic gates and circuits. To the best of our knowledge, this is the first report on reversible multiple state-switching of **1** both chemically and electrochemically. The optical read-out is fast and non-destructive, while electrochemical aspects demonstrate redox stability and electro-chromic reversibility of **1**. This study

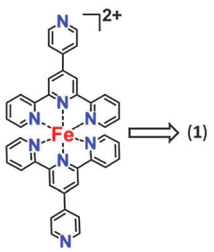

Fig. 1 Structure of the Fe-terpyridyl complex (**1**).

[a] *Department of Chemistry, University of Delhi, Delhi-110007, India. E-mail: mondalpc@gmail.com, vikram.singh19@yahoo.co.in*
[b] *Department of Chemical Physics, Weizmann Institute of Science, Rehovot-7610001, Israel*

† Dedicated to Late Dr. Tarkeshwar Gupta.

‡ Electronic supplementary information (ESI) available. See DOI: 10.1039/c4nj00121d

could possibly be an addition to the further development of solution based molecular logic gates.

2 Experimental

2.1 Materials

2-Acetyl pyridine, pyridine-4-carboxaldehyde, $FeCl_2$, NH_4PF_6, $NOBF_4$, CD_3CN, $CDCl_3$ were purchased from Sigma-Aldrich and used as received. Hydrochloric acid (HCl), triethyl amine (Et_3N) were purchased from s. d. fine chemicals (Mumbai, India). Tetra-*n*-butyl ammonium hexafluorophosphate ($TBAPF_6$) was purchased from Alfa-Aesar and it was further recrystallized and dried under vacuum before use. All other chemicals were used as received without any further purification. All solvents (AR grade) were purchased from Merck (Mumbai, India) and s. d. fine chemicals (Mumbai, India) and were purified using literature procedures so as to make them moisture free, and were further degassed using N_2 and kept in a N_2 filled glove box ($O_2 < 2$ ppm).

2.2 Physical measurements

UV-Vis spectra were recorded at room temperature on a double beam JASCO (Model V-670) spectrophotometer. A one cm path length quartz cuvette with a Teflon stopper was used for data collection. Suitable baselines were recorded for preliminary adjustments. ^{1}H NMR spectra were recorded on a JEOL 400 NMR (JNMECX 400P) using a suitable deuterated solvent. ESI-TOF (electrospray-ionization, time-of-flight) mass spectra were recorded on a microTOF QII from BrukerDaltonik (Germany). Electrochemical experiments were performed using a CH Instrument (Model 660D) electrochemical Workstation equipped with a BASi bulk electrolysis three electrode cell. Cyclic voltammograms (CV) of complex **1** was recorded in dry acetonitrile with tetra-*n*-butyl ammonium hexafluorophosphate ($TBAPF_6$) as the supporting electrolyte using glassy carbon as the working electrode (WE, $\sim$0.2 cm^2), Pt wire as the counter electrode and Ag/AgCl (in 1 M KCl) as the reference electrode (RE). For bulk electrolysis with coulometry experiments a similar procedure was followed except that porous glassy carbon (coil) was used as the working electrode (50 mm high, 5 mm thick, 40 mm diameter; surface area = 10.5 cm^2 cm^{-2}). The $TBAPF_6$ was dried at 100 °C for 30 min before use. The solution was degassed by bubbling N_2 for at least 15 min before the experiment. All the experiments were performed at room temperature unless mentioned otherwise.

2.3 Methods

Synthesis of 4′-pyridyl-2,2′:6′,2″-terpyridine (pytpy) (Scheme S1, ESI‡). pytpy was synthesized following a published procedure[23] resulting in needle shaped white crystals. ^{1}H NMR (400 MHz, $CDCl_3$): δ/ppm (Fig. S1, ESI‡) 8.76 (s, 2H), 8.78 (d, 2H), 8.68 (d, 2H), 7.8 (d, 2H), 7.89 (t, 2H), 8.75 (d, 2H), 7.39 (t, 2H); ESI-MS: *m*/*z* 310 [M^+]; UV-Vis in $CHCl_3$ (λ_{max}): 316, 278 and 245 nm.

Synthesis of 1 (Scheme S2, ESI‡). **1** was prepared according to a reported procedure.[16] In brief, 4′-pyridyl-terpyridine (98 mg; 0.316 mmol) was dissolved in 10 mL of hot methanol and then $FeCl_2$ (21 mg; 0.158 mmol) in 10 mL methanol was added dropwise. The reaction mixture was refluxed with stirring for 4 h under a N_2 atmosphere. Subsequently, the reaction mixture was slowly cooled to room temperature and **1** was precipitated out by addition of an excess of a saturated methanolic solution of NH_4PF_6, which was then filtered off. The residue was washed with an excess amount of water followed by diethyl ether and recrystallized using a mixture of acetonitrile and acetone (1 : 1, v/v) resulting in a purple colour microcrystalline solid. ^{1}H NMR (400 MHz, CD_3CN); δ/ppm (Fig. S2, ESI‡): 9.20 (s, 4H, Ar H), 9.02 (d, J = 8.0 Hz, 4H), 8.61 (d, J = 11 Hz, 4H), 8.23 (d, J = 10.2 Hz, 4H), 7.90 (t, J = 8.2 Hz, 4H), 7.15 (d, J = 5.8 Hz, 4H), 7.10 (t, J = 7 Hz, 4H). ^{13}C NMR (400 MHz, CD_3CN, δ): 118.29, 122.58, 122.98, 125.04, 128.36, 139.82, 148.75, 152.08, 154.22, 158.77, 161.84. IR, (KBr): ν = 838 (vs), 1408 (m) 1598 cm^{-1} (m). UV-Vis (CH_3CN): λ_{max} (ε) = 569 nm (23 000); ESI-TOF *m*/*z* (%): 338 (90) $[M\text{-}2PF_6]^{2+}$, 339 (46) $[(M\text{-}2PF_6) + H^+]^{2+}$, 821(30) $[(M\text{-}PF_6)]^+$, anal. calcd. for $C_{40}H_{28}N_8FeP_2F_{12}$: C, 45.47; H, 3.63; N, 10.61. Found: C, 45.16; H, 3.34; N, 9.96%.

2.4 Preparation of solutions of 1 and other chemical reagents

A 10 μM solution of **1** was prepared in CH_3CN (purple coloured solution) and kept inside a N_2 glove box and is pipetted out as and when required. The complex solution was sufficiently stable in the presence of air/light within the experimental time-frame. 100 ppm of a fresh $NOBF_4$ (source of NO^+) solution in dry CH_3CN was prepared, as per requirement, for further dilution to one and two eq. solutions with respect to **1**. Conc. HCl and Et_3N were diluted to one and two eq. with respect to **1**, using deionized water.

2.5 Chemical induced optical switching

Optical changes in 1 induced by NO^+ and H^+. At first, the UV-Vis spectrum of 2 mL of 10 μM solution of **1** was recorded in transmission mode in the 200–800 nm range with CH_3CN for baseline correction. (*Note: any external chemical added afterwards was added to both the sample and reference so as to measure optical changes occurring for **1** only*). One eq. of freshly prepared NO^+ solution was then added using a 0 to 200 μL pipette and the corresponding UV-Vis spectrum was recorded. Then another equivalent of NO^+ was added and the UV-Vis spectrum was recorded thereafter. Furthermore, in a separate experiment, an excess of NO^+ (>2 eq.) was added and corresponding changes in the UV-Vis spectrum were recorded. A similar procedure was followed for addition of HCl solution. All additions and recording optical absorption were performed under standard conditions.

For switching back optical changes in 1. To the **1** + NO^+ (excess) solution, 5 μL of deionized water and two equivalents of Et_3N were added in a stepwise manner with recording of the UV-Vis spectrum at each step. To the **1** + H^+ solution two equivalents of Et_3N was added and its UV-Vis spectrum was recorded.

2.6 Spectro-electrochemical switching

At first, the cyclic voltammogram of 10 μM of **1** in dry CH_3CN was recorded with 20 mM $TBAPF_6$ as the supporting electrolyte. The Fe(II)/Fe(III) couple was observed at ΔE_{pa} = 1.24 V and ΔE_{pc} = 1.17 V with $E_{1/2}$ = 1.20 V at a scan rate of 0.3 V s^{-1}. Now, with a similar concentration of **1** bulk electrolysis was performed by coulometry at an initial potential of 1.4 V, so as to oxidise **1**. At an interval of 500 s, 2 mL of solution was drawn from the electrolytic cell and its optical absorption was recorded and the process was continued till there was no further alteration in the optical absorption or when the increase in charge saturates with respect to time. For Fe(III) to Fe(II) conversion, a potential of 1.0 V was applied and a similar procedure was followed thereafter. The UV-Vis spectrum was recorded after considering $TBAPF_6$ solution in CH_3CN as baseline for preliminary adjustments.

2.7 Molecular computational studies

The ground state geometry optimizations of $\mathbf{1}^{2+}$, $\mathbf{2}^{3+}$, $\mathbf{3}^{4+}$ and $\mathbf{4}^{5+}$ were carried out in the gas phase using the B3LYP method and the LANL2DZ[24,25] basis set with an effective core potential was used for the iron atom. The 6-31G*[26] basis set was used for all other atoms except iron. The initial geometry was obtained from the standard geometrical parameters. All calculations were performed using the Gaussian 03 program package.[27]

3 Results and discussions

3.1 Optical monitoring of switching events

Fe(II)-terpyridiyl complexes characteristically exhibit a ^{1}MLCT band in the visible region of the spectrum, whose peak position is obviously dependent on the ligand environment, while Fe(III) analogues generally lack this characteristic.[21] Moreover, interconversion of the two oxidation states could be performed using suitable oxidizing/reducing agents. Particularly, addition of water could easily convert Fe(III) to Fe(II). In the case of **1**, the MLCT band appeared at λ_{max} = 569 nm in dry CH_3CN. Additionally, the free pendant pyridyl groups of **1** could potentially interact or form adducts with several cationic species, including NO^+ and H^+, due to the presence of non-bonding electrons on the N-atom.[28]

Chemical inputs induced optical changes. The optical and structural attributes of state-switching of **1** were obtained by using carefully chosen chemical input(s) applied at different stages of the switching experiment, *viz.* NO^+, H^+, H_2O and Et_3N. Addition of one eq. of NO^+ to **1** shifted the ^{1}MLCT band peak position to 586 nm (+17 nm shift) along with a visible, instant colour change to light purple/blue (Fig. 2($\mathbf{2}^{3+}$)). Another eq. of NO^+ further shifted the ^{1}MLCT band to 590 nm (+4 nm shift) and the colour of the solution changed to blue (Fig. 2($\mathbf{3}^{4+}$)). Moreover, optical absorption of the ^{1}MLCT band increased with each addition step as signified by 13% and 34% increases in molar absorptivity ('ε') for each addition, respectively. Addition of excess of NO^+ (>2 eq.) to **1** produced remarkable deviation from the above behaviour. With each further aliquot (1 eq. each), the ^{1}MLCT band centred at λ_{max} = 590 nm started to diminish in intensity, finally resulting in a broad band in the range ~600–800 nm and a concomitant blue to green colour change (Fig. 2($\mathbf{4}^{5+}$)).

Explanation and verification of observed changes. The most plausible explanation for observed bathochromic and hyperchromic shifts in optical absorption spectra of **1** upon addition

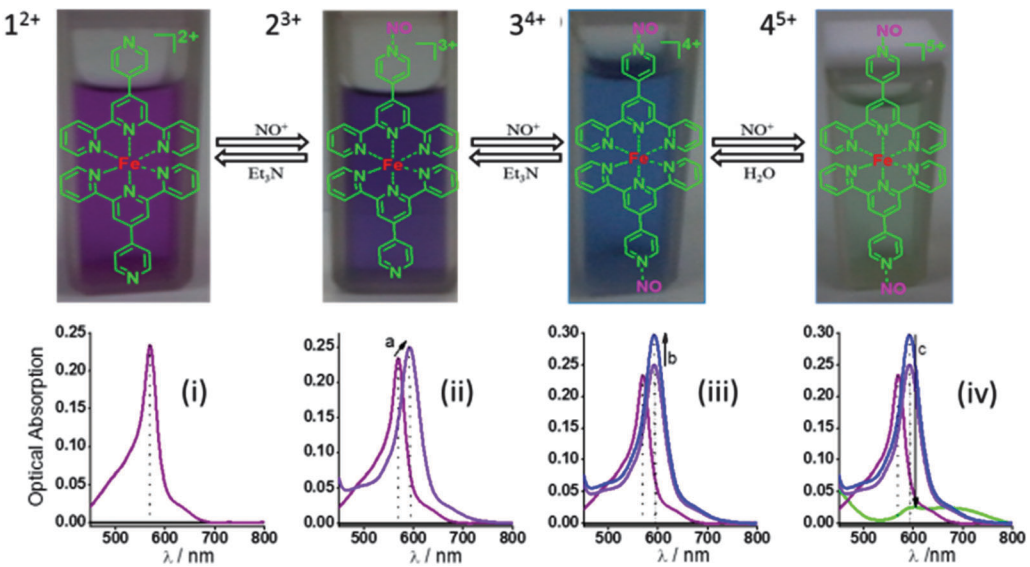

Fig. 2 (i) Native colour of **1** in CH_3CN and (below) the corresponding UV-Vis spectrum (^{1}MLCT) with λ_{max} = 569 nm; (ii) addition of 1 eq. of NO^+ to **1** with a colour change from purple to blue and (below) 'a' represents bathochromic shift of 17 nm to 586 nm and an increase in the molar absorptivity in ^{1}MLCT of **1**; (iii) addition of another eq. of NO^+ to **1** changed the colour to light blue and (below) 'b' represents changes in the UV-Vis spectrum; (iv) excess of NO^+ results in green colour and (below) 'c' represents vanishing of ^{1}MLCT leading to Fe^{3+} formation. Successive use of H_2O and Et_3N leads to the original state of **1**. The black line in the UV-Vis spectra represents baseline with dry CH_3CN.

of NO^+ could potentially be the sequential quaternization of pendant pyridyl N-atoms. Induced electron deficiency in the terpyridyl unit forces it to withdraw electronic charge from the metal centre. This perhaps resulted in lowering of the band gap between metal and ligand centred molecular orbitals and hence bathochromism is observed.[21] Hyperchromic effects at fixed concentrations are generally related to the increase in 'ε'. Formation of different species from **1** could only bring about changes in 'ε'. The concept of quaternization is based on the fact that the ionization energy of the appended pyridine unit is slightly greater than that of NO and consequently the charge transfer process (pyridyl N-atom to NO^+ or Fe(II) to NO^+) is inhibited to a large extent and adduct formation prevails.[28–30] The probable absence of quaternization sites for further added aliquots of NO^+ makes the charge transfer from the metal centre Fe(II) to NO^+ the most reasonable conclusion, ably supported by the diminishing ^{1}MLCT band, appearance of a broad band in the range ~600–800 nm and visible colour change. This potentially signifies the oxidation of Fe(II) to Fe(III).[31] Moreover, absence of H_2O and O_2 in CH_3CN rules out the probable formation of acid (HBF_4) and protonation of pyridyl N-atoms upon reaction with HBF_4. To further verify that adduct formation governs the process, dil. HCl was added to a solution of **1** and the UV-Vis spectrum was recorded (Fig. S3, ESI‡). Upon addition of one eq. of dil. HCl, the colour changed to light purple and the ^{1}MLCT band peak position shifted to 582 nm (+13 nm shift) and 'ε' was enhanced by 10% (Fig. S3(2), ESI‡). Addition of two equivalents of dil. HCl produced blue colour and the ^{1}MLCT band peak position shifted to λ_{max} = 590 nm with a net 26% increase in 'ε' (Fig. S3(3), ESI‡). Further addition of equivalents of dil. HCl did not induce any further spectral or colour changes in **1**. These spectral changes could well be ascribed to the protonation of pendant pyridyl N-atoms.[32] We observed a significant difference in addition of NO^+ and H^+ to **1**: changes in molar absorptivity, '$\Delta\varepsilon$', in the case of addition of NO^+ are greater than that with addition of H^+. 'ε' is the intrinsic property of a species. If there had been no adduct formation between **1** and NO^+ (A; see below), the species generated in both cases would probably have been the same ($-C_5H_4N^+$) (B; see below) and $\Delta\varepsilon$ values similar, which is not the case. Thus, it is tentatively stated that NO^+ leads to adduct formation, while H^+ promotes charge transfer.

$$NO^+ + -C_5H_4N \rightarrow \underset{A}{NO^{+\bullet}} + -C_5H_4N + \underset{B}{-C_5H_4N^+} + NO$$

Reverting to the original optical signal. In continuation, addition of only 5 μL of deionized H_2O to a NO^+ saturated solution of **1** resulted in quick reappearance of the ^{1}MLCT band at λ_{max} = 590 nm and change of the colour to blue from green (Fig. S4(1), ESI‡). Further addition of H_2O neither resulted in reposition of the ^{1}MLCT band to the original value of λ_{max} = 569 nm nor produced any colour change or change in 'ε' value. This suggested that addition of H_2O induced possible reduction of Fe(III) to Fe(II), which is actually a well-known phenomenon, but failed to dequaternize the adduct forming pyridyl N-atoms as proposed earlier (dicationic species). Moreover, the dicationic species (adduct) could be considered as a weak Lewis acid and it was presumed that action of a mild Lewis base such as Et_3N would neutralize as well as dequaternize the pyridyl N-atoms. This was indeed what we observed after addition of two eq. of Et_3N solution to the solution of dicationic species. The ^{1}MLCT band reverted to λ_{max} = 569 nm along with an instant change in colour from blue to purple (Fig. S4(2), ESI‡). Addition of water to the **1** + H^+ solution produced no effect, while addition of 2 eq. of Et_3N restored the ^{1}MLCT peak position. To check the effect of direct addition of either H_2O or Et_3N to **1**, control experiments were performed. 2 eq. each of H_2O and Et_3N were added either individually or together to a solution of **1**, but no noticeable change was observed even after 30 min of reaction.

Thus, **1** could exist in four stable states formed stepwise, *viz.* monocationic, dicationic, dicationic-oxidized and **1** itself, upon careful sequential addition of NO^+. Additionally, monoprotonated and bisprotonated states were observed in the case of addition of H^+. Moreover, facile switching between different states could be achieved by addition of selected chemical reagents as input. This behaviour of **1** prompted its use as a molecular switch, as the different molecular states were inter-convertible as well as stable within the experimental time-frame. Moreover, the whole exercise was repeated at least ~4 times to confirm the switching behaviour using the same solution of **1**. Fig. 3 (left panel) demonstrates the effect of set–reset events on optical absorption at λ_{max} = 590 nm for addition of NO^+ to **1**. It does not include the action of Et_3N. With each cycle, there was only ~5–8% signal loss (change in optical absorption) at each step of switching from **1** to the dicationic-oxidized state and back, which could be termed as reasonable performance in terms of efficiency. Similar signal losses were observed for addition of H^+. Moreover, signal deviation from three independent switching experiments with different solutions of **1** (10 μM each) was only ~3–6%, (Fig. 3, right panel) which potentially indicates the sufficient accuracy of the multiple switching events.

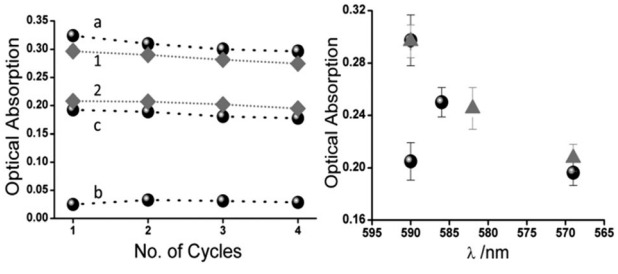

Fig. 3 Black spheres represent addition of NO^+ and grey squares addition of H^+. (left) Optical switching of the same solution of **1** across four cycles. 'a' indicates changes in absorbance of the dicationic state for a single solution in four cycles. Similarly 'b' and 'c' indicate changes in absorbance of the oxidized and original state after regeneration respectively. '1' and '2' indicate changes in absorbance of the bisprotonated and original state after regeneration respectively. Overall, ~5–8% signal loss was observed after four cycles. (right) ~3–6% deviation in absorbance of **1** at different wavelengths under study, after addition of either NO^+ or H^+ in three separate experiments. Dotted lines are guide to eyes.

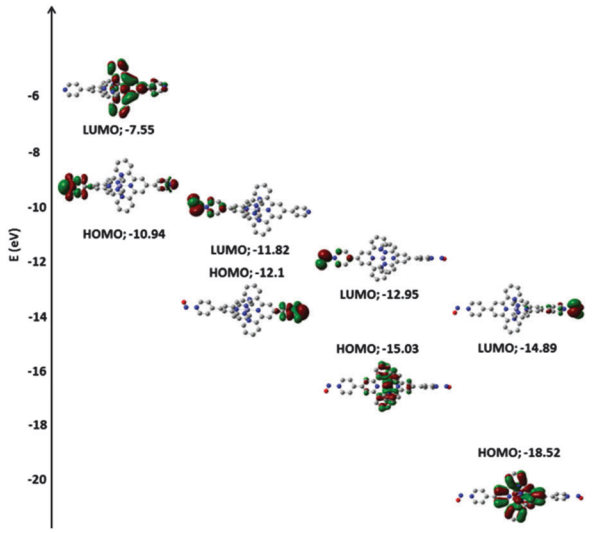

Fig. 4 Molecular orbital pictures (HOMO and LUMO) of $\mathbf{1}^{2+}$, $\mathbf{2}^{3+}$, $\mathbf{3}^{4+}$ and $\mathbf{4}^{5+}$ in the gas phase.

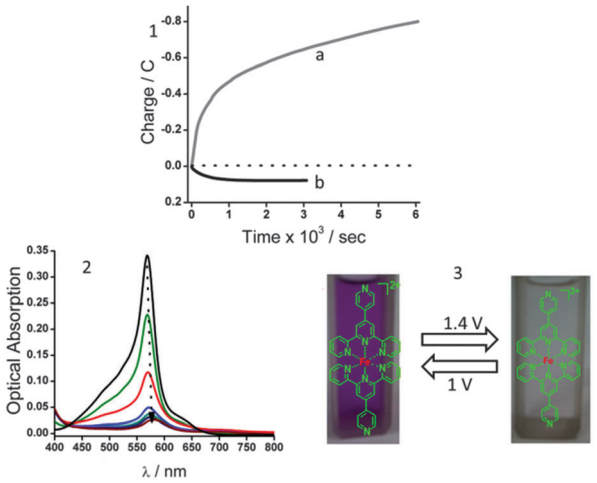

Fig. 5 (1) Bulk electrolysis with coulometry of **1** in CH_3CN. 'a' represents oxidation of **1** at an applied potential of 1.4 V while 'b' signifies reduction of **1** from the oxidized state at an applied potential of 1.0 V; (2) corresponding changes in the UV-Vis spectrum of **1** during electrochemical oxidation and (3) visual colour changes upon application of potential.

3.2 Properties of molecular orbitals

DFT studies revealed that the highest occupied molecular orbital (HOMO) of $\mathbf{1}^{2+}$ and $\mathbf{2}^{3+}$ is dominated by the pyridyl moiety of pytpy (see Fig. S5a–d for optimized structures and Tables S1 and S2 for selected bond lengths and angles, ESI‡). On the other hand, in the HOMO of $\mathbf{3}^{4+}$ and of $\mathbf{4}^{5+}$ the electronic charge density is mainly distributed over metal d orbitals and the pyridyl unit. It is observed that for all different states of **1**, lowest unoccupied molecular orbitals (LUMO's), electron densities are predominantly residing on pytpy moiety. For the corroboration of experimentally observed results, calculation of HOMO–LUMO energy gaps was performed ($\mathbf{1}^{2+}$ for 3.39 eV, $\mathbf{2}^{3+}$ for 0.28 eV, $\mathbf{3}^{4+}$ for 2.08 eV and $\mathbf{4}^{5+}$ for 3.63 eV), which is in general agreement with the changes observed in the ^{1}MLCT band of **1** upon addition of NO^+ (Fig. 4).

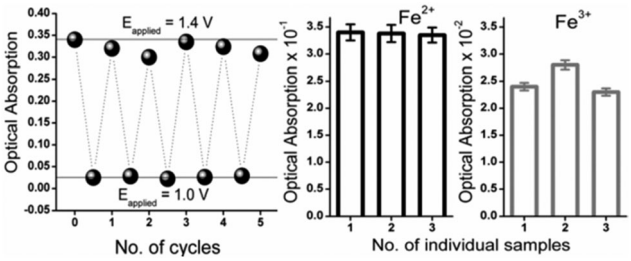

Fig. 6 (left) Changes in absorbance of **1** in CH_3CN upon application of potential across five cycles for a single sample resulting in ~5% signal loss. Top sphere to bottom sphere: $E_{applied}$ = 1.4 V; bottom to top sphere: $E_{applied}$ = 1.0 V. (right) Signal deviation of ~4–6% (in terms of absorbance) was observed in three separate spectro-electrochemical switching events. Fe^{2+} represents the reduced state (presence of ^{1}MLCT) and Fe^{3+} the oxidized state (absence of ^{1}MLCT). Dotted lines are guide to eyes.

3.3 Spectro-electrochemical switching events

During bulk electrolysis with coulometry, an applied potential of 1.4 V produced a significant visible change in the colour of the solution which was confirmed by reduction in the optical absorption at 569 nm. The purple colour of the solution became colourless within ~3000 s and changes in the optical absorption became stagnant at ~6000 s. This observation was in sync with the saturation of charge with respect to time and is presented in Fig. 5. At this point, the applied potential was changed to 1.0 V and the experiment was re-run. Within ~2500 s, the colour changed to purple from colourless and optical absorption was restored almost to the original level (Fig. S6, ESI‡).

The colour changes upon applied potential and as verified through UV-Vis spectroscopy could be easily attributed to Fe(II)/Fe(III) conversion based on the reversible and oxidation state dependent electrochromic effect. Moreover, in a similar experiment performed at least five times with the same solution, an ~5% signal loss was observed (Fig. 6, left panel). Furthermore, it was also observed that there was only ~4–6% signal deviation from three independent reversibility experiments each performed for at least five cycles (Fig. 6, right panel). In addition, cyclic voltammograms of **1** were recorded for 300 cycles at a scan rate of 0.3 V s^{-1} and no degradation of **1** was noticed under experimental conditions (Fig. S7, ESI‡). These experiments suggest that electrochemical switching events are sufficiently efficient and accurate along with satisfactory stability of different oxidation states of **1**.

3.4 Construction of logic gates and circuits

Based on the experimental results, we constructed two and three input molecular logic gates and circuits using **1** and the chemical inputs at the molecular level. For designing logic gates, addition of NO^+ or H^+ was considered as Input = 1, else Input = 0. Similarly, the significant optical changes were observed considered as Output = 1, else Output = 0. In the presence of H^+, the MLCT transition of **1** showed a red shift, while addition of Et_3N reconfigured the MLCT transition.

Input 1 (H^+)	Input 2 (Et_3N)	Ouput (λ_{max} = 590 nm)
0	0	0
1	0	1
0	1	0
1	1	0

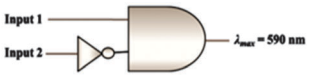

Fig. 7 Representation of the INHIBIT logic gate constructed using two inputs (H^+ and Et_3N) applied on (**1**). Given alongside is the associated truth table.

To accomplish a logic gate, addition of H^+ was considered as Input1 = 1, while addition of Et_3N as Input2 = 1, while the shifting of the MLCT band to λ_{max} = 590 nm was considered as Output = 1. When both the chemical inputs (H^+ and Et_3N) were added (Input1 and Input2 = 1) simultaneously, Output = 0 was obtained. Interestingly, when Input1 was applied, Output was observed but no Output was observed upon exclusive application of Input2. This result is presented in Fig. 7 as the INHIBIT molecular logic gate along with the truth table.

Molecular logic circuits using three chemical inputs and two outputs have also been designed using **1**. The three chemical inputs used were NO^+ (excess), Et_3N and H_2O as Input1, Input2 and Input3, respectively. The absorbance ("1" for above the threshold value, "0" for below the threshold value) and the red shift of the MLCT band to λ_{max} = 590 nm were considered as Output1 and Output2 respectively (Fig. 8). The truth table for multiple chemical inputs and multiple outputs has been presented. The Output1 was obtained for all combinations except when Input1 = 1, Input2 = 0 and Input3 = 0, while Output2 was observed ("1") exclusively when Input1 and Input3 were applied and Input2 was absent The observation afforded the three input logic circuits as presented in Fig. 9.

In summary, it has been demonstrated that **1** possess controllable multiple switching characteristic and is able to generate logic gates and circuits. The operation mechanism has also been proposed and justified. The complex showed a multiple switching event and NO^+ plays a dual role *i.e.*, quaternization at lower concentration and oxidation at higher concentration. The molecular switch in response to the external chemical inputs is capable of executing multiple binary Boolean logics at the molecular level. These attractive features make **1** a smart candidate for the development of hybrid materials[33,34] and it could potentially be used for chemically addressable information processing devices at the molecular level.[35] Notably, the above complex showed reversible color change upon applying potential so, it could potentially find application as an electrochromic material[36,37] and in molecular memory devices.[38,39]

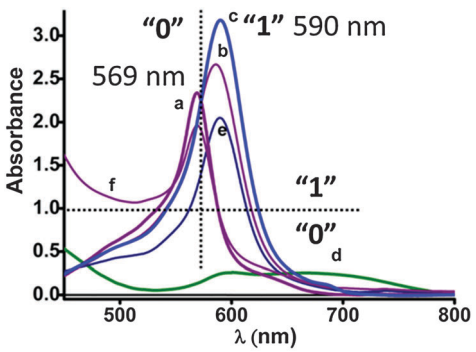

Fig. 8 Combined UV/Vis spectra of **1** undergoing switching between different reversible stable states upon external chemical stimulus. (a) MLCT band of **1** with λ_{max} = 569 nm; (b) 1 eq. of NO^+, (c) 2 eq. of NO^+, (d) excess of NO^+; (e) 5 μL of DI H_2O; (f) addition of Et_3N. The black line represents baseline with dry acetonitrile. Threshold criteria are clearly indicated.

Input 1 (NO^+)	Input 2 (Et_3N)	Input 3 (H_2O)	Output 1 (Absorbance)	Output 2 (λ_{max}590 nm)
0	0	0	1	0
0	0	1	1	0
0	1	0	1	0
0	1	1	1	0
1	0	0	0	0
1	0	1	1	1
1	1	0	1	0
1	1	1	1	0

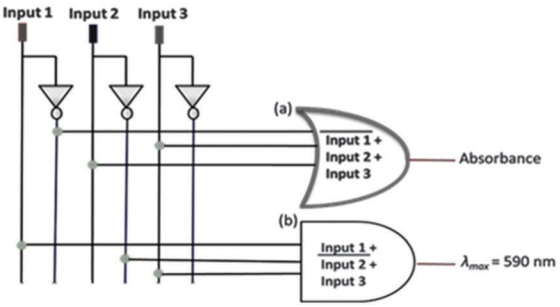

Fig. 9 Representation of molecular logic circuits constructed using three (NO^+, Et_3N, H_2O) inputs and resulting in two outputs. Given alongside is the associated truth table.

Acknowledgements

PCM and VS thank Council of Scientific and Industrial Research and University Grants Commission (New Delhi, India), respectively, for Senior Research Fellowship. The authors would like to thank the reviewers for their fruitful suggestions.

Notes and references

1 G. de Ruiter and M. E. van der Boom, *Acc. Chem. Res.*, 2011, **44**, 563.
2 G. de Ruiter and M. E. van der Boom, *Angew. Chem., Int. Ed.*, 2010, **122**, 173.
3 S. J. Langford and T. Yann, *J. Am. Chem. Soc.*, 2003, **125**, 11198.
4 U. Pischel, *Angew. Chem., Int. Ed.*, 2007, **46**, 4026.
5 P. Ball, *Nature*, 2000, **406**, 118.
6 V. Balzani, A. Credi, F. M. Raymo and J. F. Stoddart, *Angew. Chem., Int. Ed.*, 2000, **112**, 3484.
7 R. F. Service, *Science*, 2001, **293**, 785.

8 D. A. Muller, T. Sorsch, S. Moccio, F. H. Baumann, K. Evans-Lutterodt and G. Timp, *Nature*, 1999, **399**, 758.
9 T. Gupta and M. E. van der Boom, *Angew. Chem., Int. Ed.*, 2008, **120**, 5402.
10 M. Grätzel, *Nature*, 2001, **414**, 338.
11 G. J. Samuels and T. J. Meyer, *J. Am. Chem. Soc.*, 1981, **103**, 307.
12 A. P. de Silva, *Nature*, 2008, **454**, 417.
13 S. Weng, W. Shen, Y. Feng and H. Tian, *Chem. Commun.*, 2006, 1497.
14 F. M. Raymo and S. Giordani, *J. Am. Chem. Soc.*, 2001, **123**, 4651.
15 S. Erbas-Cakmak and E. U. Akkaya, *Angew. Chem., Int. Ed.*, 2013, **52**, 11364.
16 S. Erbas-Cakmak, O. A. Bozdemir, Y. Cakmak and E. U. Akkaya, *Chem. Sci.*, 2013, **4**, 858.
17 S. Bi, B. Ji, Z. Zhang and J.-J. Zhu, *Chem. Sci.*, 2013, **4**, 1858; K. S. Hettie, J. L. Klockow and T. E. Glass, *J. Am. Chem. Soc.*, DOI: 10.1021/ja501211v.
18 D. C. Magri, M. C. Fava and C. J. Mallia, *Chem. Commun.*, 2014, **50**, 1009.
19 F. Pu, E. Ju, J. Ren and X. Qu, *Adv. Mater.*, 2014, 26.
20 V. Singh, P. C. Mondal, J. Y. Lakshmanan, M. Zharnikov and T. Gupta, *Analyst*, 2012, **137**, 3216.
21 P. C. Mondal, J. Y. Lakshmanan, H. Hamoudi, M. Zharnikov and T. Gupta, *J. Phys. Chem. C*, 2011, **115**, 16398.
22 T. Gupta, P. C. Mondal, A. Kumar, Y. L. Jeyachandran and M. Zharnikov, *Adv. Funct. Mater.*, 2013, **23**, 4227.
23 A. Winter, A. M. J. van der Berg, R. Hoogenboom, G. Kickelbick and U. S. Schubert, *Synthesis*, 2006, 2873.
24 M. M. Francl, W. J. Pietro, W. J. Hehre, J. S. Binkley, D. J. DeFrees, J. A. Pople and M. S. Gordon, *J. Chem. Phys.*, 1982, **77**, 3654.
25 V. A. Rassolov, M. A. Ratner, J. A. Pople, P. C. Redfern and L. A. Curtiss, *J. Comput. Chem.*, 2001, **22**, 976.
26 W. R. Wadt and P. J. Hay, *J. Chem. Phys.*, 1985, **82**, 284.
27 M. J. Frisch, G. W. Trucks, H. B. Schlegel, G. E. Scuseria, M. A. Robb, J. R. Cheeseman, J. A. Montgomery Jr., T. Vreven, K. N. Kudin, J. C. Burant, J. M. Millam, S. S. Iyengar, J. Tomasi, V. Barone, B. Mennucci, M. Cossi, G. Scalmani, N. Rega, G. A. Petersson, H. Nakatsuji, M. Hada, M. Ehara, K. Toyota, R. Fukuda, J. Hasegawa, M. Ishida, T. Nakajima, Y. Honda, O. Kitao, H. Nakai, M. Klene, X. Li, J. E. Knox, H. P. Hratchian, J. B. Cross, C. Adamo, J. Jaramillo, R. Gomperts, R. E. Stratmann, O. Yazyev, A. J. Austin, R. Cammi, C. Pomelli, J. W. Ochterski, P. Y. Ayala, K. Morokuma, G. A. Voth, P. Salvador, J. J. Dannenberg, V. G. Zakrzewski, S. Dapprich, A. D. Daniels, M. C. Strain, O. Farkas, D. K. Malick, A. D. Rabuck, K. Raghavachari, J. B. Foresman, J. V. Ortiz, Q. Cui, A. G. Baboul, S. Clifford, J. Cioslowski, B. B. Stefanov, G. Liu, A. Liashenko, P. Piskorz, I. Komaromi, R. L. Martin, D. J. Fox, T. Keith, M. A. Al-Laham, C. Y. Peng, A. Nanayakkara, M. Challacombe, P. M. W. Gill, B. Johnson, W. Chen, M. W. Wong, C. Gonzalez and J. A. Pople, *Gaussian 03, Revision B.03*, Gaussian, Inc., Pittsburgh, PA, 2003.
28 P. Spanel and D. Smith, *Int. J. Mass Spectrom.*, 1998, **176**, 203.
29 K. Y. Lee, D. J. Kuchynka and J. K. Kochi, *Inorg. Chem.*, 1990, **29**, 4196.
30 K. J. Adaikalasamy, N. S. Venkataramanan and S. Rajagopal, *Tetrahedron*, 2003, **59**, 3613.
31 E. Z. Jandrasics and F. R. Keene, *J. Chem. Soc., Dalton Trans.*, 1997, 153.
32 M. G. Lobello, S. Fantacci, A. Credi and F. D. Angelis, *Eur. J. Inorg. Chem.*, 2011, 1605.
33 P. C. Mondal, B. Gera and T. Gupta, *Advanced Organic-Inorganic Composites: Materials Device and Allied Applications*, Nova Science Publishers, Inc., USA, 2012, ch. 2, p. 33.
34 O. Shekhah, J. Liu, R. A. Fischer and C. Wöll, *Chem. Soc. Rev.*, 2011, **40**, 1081.
35 D. Cotter, R. J. Manning, K. J. Blow, A. D. Ellis, A. E. Kelly, D. Nesset, I. D. Phillips, A. J. Poustie and D. C. Rogers, *Science*, 1999, **286**, 1523.
36 L. Motiei, M. Lahav, D. Freeman and M. E. van der Boom, *J. Am. Chem. Soc.*, 2009, **131**, 3468.
37 M. Li, A. Patra, Y. Sheynin and M. Bendikov, *Adv. Mater.*, 2009, **21**, 1707.
38 P. C. Mondal, *Adv. Energy Mater.*, John Wiley & Sons, Inc., Hoboken, NJ, USA, 2014, ch. 13, p. 499.
39 A. Kumar, M. Chhatwal, P. C. Mondal, V. Singh, A. Gulino and R. D. Gupta, *Chem. Commun.*, 2014, **50**, 3783.